Available online at www.sciencedirect.com
ScienceDirect
International Journal of Heat and Mass Transfer 50 (2007) 4011–4022
International Journal of HEAT and MASS TRANSFER
www.elsevier.com/locate/ijhmt

Cryogenic chilldown process under low flow rates

Kun Yuan, Yan Ji, J.N. Chung *

Department of Mechanical and Aerospace Engineering, University of Florida, Gainesville, FL 32611-6300, USA

Received 22 June 2006; received in revised form 26 January 2007
Available online 5 April 2007

Abstract

In this paper, we investigated the chilldown process of a horizontal tube by a liquid nitrogen flow with low mass fluxes. The flow patterns and heat transfer characteristics are studied experimentally. Visualization results illustrate the successive states of liquid–wall interaction with different mass fluxes. For a horizontal tube, the liquid filament–wall interaction is an important contributor to the heat transfer on the bottom wall while the upper wall is cooled by forced convection with superheated vapor. A phenomenological model is developed, in which the heat transfer on the bottom wall is composed of film boiling and forced convection while for the upper wall, forced convection is the only mechanism of heat transfer. A good agreement is achieved between the model prediction and the experimental result.

Keywords: Chilldown; Quenching; Dispersed flow; Film boiling; Heat transfer; Cryogenic

1. Introduction

Cryogenic fluids are widely used in industrial systems, aerospace systems, cryosurgery systems and, etc. In these systems, proper transport, handling and storage of cryogenic fluids are of great importance. Chilldown or quenching process is the initial stage of cryogenic fluid transport. It is a complicated process involving unsteady two-phase heat and mass transfer.

The pioneer study on cryogenic chilldown process was conducted by Burke et al. [1] and Bronson et al. [2]. Chilldown of a large pipe system, from 15 to 50 m long, with liquid nitrogen or liquid hydrogen was investigated in their work. The detail of the flow regime and heat transfer characteristic was, however, lacking in their research. Antar and Collins [3] investigated the chilldown of a vertical tube by injecting liquid nitrogen from the bottom under both terrestrial and low gravity environment. Two different test sections were used; a quartz tube was used for visualizing the flow regime while a stainless steel tube was used for temperature measurement. As a consequence, it is hard to associate the visualized flow regime with the measured wall temperature. To evaluate the loss of coolant accident (LOCA) in a boiling water reactor, a series of quenching studies was conducted by Rohsenow et al. [4–7] and they dealt with both inverted annular and dispersed flow boiling of liquid nitrogen in a vertical pipe.

To avoid the experimental difficulty of using cryogens, some researchers used other common fluids to study the chilldown process. For example, Chan and Banerjee [8] used water to quench a hot horizontal tube under different initial and boundary conditions. Westbye et al. [9] used R-113 in the quenching test of a horizontal tube under both terrestrial and microgravity conditions.

Despite the different working conditions and test section designs used by the previous researchers, the mass fluxes in those tests were generally higher than 40 kg/m^2s. For example, the liquid nitrogen mass fluxes in the experiments of Antar and Collins [3] were in the range of 550–1940 kg/m^2s and they were 40.7–271.3 kg/m^2s in the experiments of Iloeje et al. [7], while the mass fluxes of R-113 used by Westbye et al. [9] were from 160 to 850 kg/m^2s. However, no experimental work has been reported for the cryogenic chilldown process at relatively lower mass fluxes.

* Corresponding author. Tel.: +1 352 392 9607; fax: +1 352 392 1071.
E-mail address: jnchung@ufl.edu (J.N. Chung).

0017-9310/$ - see front matter © 2007 Elsevier Ltd. All rights reserved.
doi:10.1016/j.ijheatmasstransfer.2007.01.034

Nomenclature

C_{pg}	specific heat capacity of the gas in the vapor film [J/kg K]
D	diameter of the flow channel [m]
F_L	time averaged fraction of bottom wall surface that is associated with liquid filaments
g	gravitational acceleration constant [m/s^2]
h_{lg}	latent heat of evaporation [J/kg K]
h'_{lg}	latent heat plus vapor sensible heat content [J/kg K]
k	thermal conductivity [W/m K]
Pr	Prandtl number
q''	heat flux [W/m^2]
R	radius of the flow channel [m]
Re_D	Reynolds number
T	temperature [K]
ΔT_w	wall superheat [K]

Greek symbols

δ	vapor film thickness [m]
δ_0	bottom wall vapor film thickness [m]
ρ	density [kg/m^3]

Subscripts

b	bottom wall
conv	convection
fb	film boiling
g	gas in the vapor film
l	liquid phase
max	maximum
min	minimum
sat	saturation
u	upper wall
v	vapor phase
w	wall

The present investigation is driven by the need for a further understanding of the cryogenic chilldown process at low mass fluxes, which has potential application in the thermodynamic vent system (TVS) on a spacecraft. A TVS is a system where a small amount of liquid is withdrawn from a cryogenic propellant tank and allowed to vaporize to remove heat from the bulk liquid cryogen in the tank and thus lower the tank pressure [10]. The mass flux in a TVS is generally very low. Van Dresar et al. [11,12] conducted systematic experiments on studying the heat transfer characteristics and flow regimes of two-phase nitrogen and hydrogen flows. In their tests the mass flux for nitrogen ranged from 3.3 to 33 kg/m^{2}s. Their experiments were conducted under a steady state. The highly transient chilldown process was not included. In this paper, a horizontal tube is quenched by a gravity driven flow and a bellow driven flow, respectively, with mass fluxes ranging from 3.6 to 10.8 kg/m^{2}s. The flow regimes and heat transfer behavior are studied experimentally. In order to observe a complete chilldown process and obtain a boiling curve, the gravity driven flow is designed. The bellows driven flow experiment is specially used to study the heat transfer behavior during the film boiling regime. A phenomenological model is developed based on this experimental observation.

2. Experimental program

2.1. Apparatus

A compact experimental system was designed as a once-through flow pass using a motor-driven bellows as the flow generator. Fig. 1 shows a schematic of the experimental system, which is located in two side-by-side aluminum cubicles. The experimental system mainly consists of a nitrogen tank, a motor-driven bellows, test section inlet portion, test section, test section outlet portion, a vacuum jacket, a vacuum pump, a data acquisition system, and a lighting and video system.

Following the traditional method to control the cryogenic flow [11–13], a nitrogen flow was generated by a motor-driven stainless steel bellows. The bellows was submerged in the liquid nitrogen inside a nitrogen tank. When the motor was turned on, the bellows would be compressed at a constant speed. Before introduce the nitrogen flow to the test section, the feeding of the bellows and the tank is repeated several times to ensure that the entire flow delivery system is at a quasi-steady state. When the bellows is full, the pull rods are pulled to compress and drive out possible nitrogen vapor at the top of the bellows and then the bellows are fed again, this process is also repeated several times. Therefore, we believe the exit flow is pure liquid. The bellows-driven system serves as both a flow generator and a flow measurement device. Three different motor speeds were used in the test which resulted in mass fluxes from 3.6 to 10.8 kg/m^{2}s.

The test section was a transparent pyrex glass tube with an OD of 15.8 mm, ID of 11.1 mm and length of 254 mm. There were 9 small holes drilled along the test section at three different cross sections. On each cross section, there were three holes separated at 120° apart from one another circumferentially. The depth of the holes was 2.0 mm. For temperature measurement, a total of 15 type-T thermocouples were

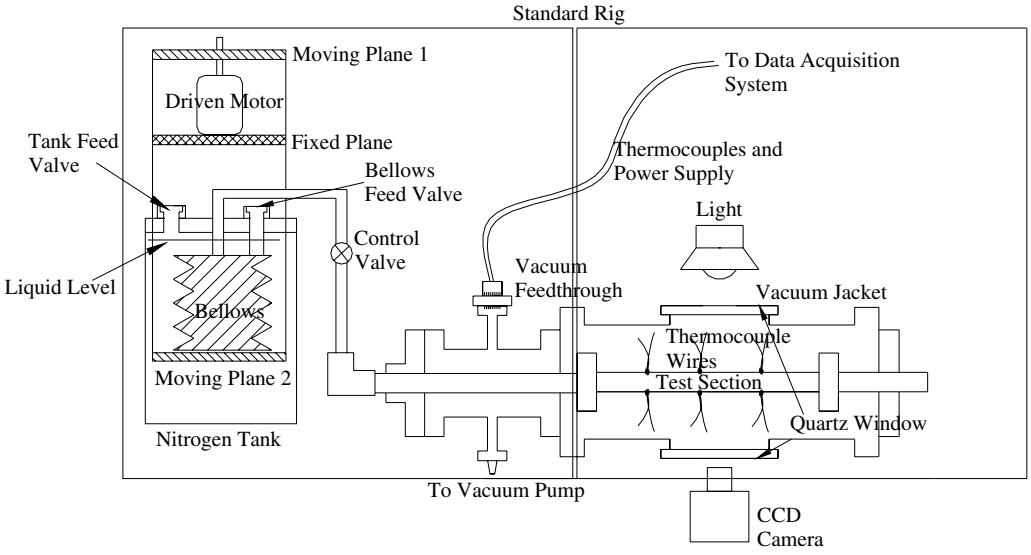

Fig. 1. Schematic of cryogenic chilldown test apparatus.

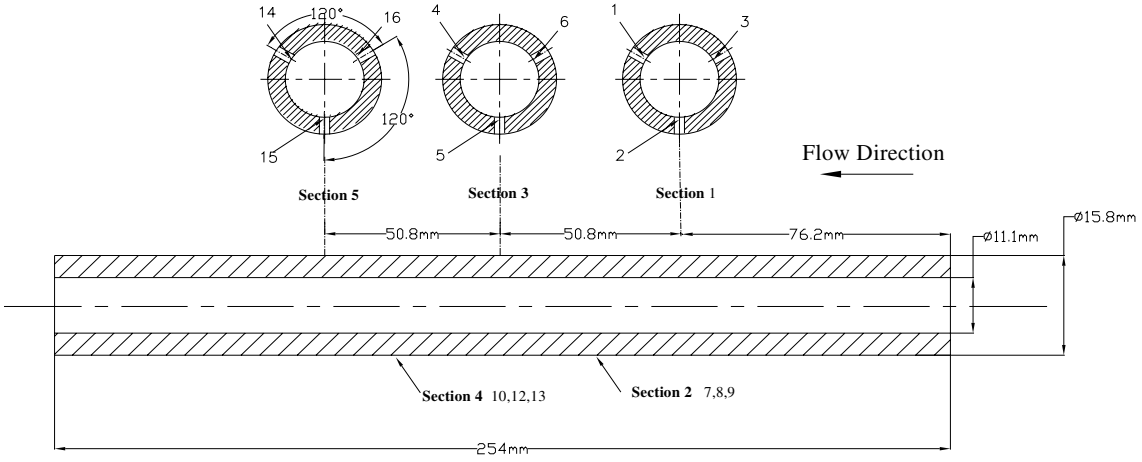

Fig. 2. Sketch of the test section and thermocouple locations.

used. Nine thermocouples were imbedded into the small holes and the other six thermocouples were used to record the outside wall temperature. The sketch of the test section and the thermocouple arrangement are shown in Fig. 2.

The test section inlet, test section and test section outlet were placed inside of a stainless steel vacuum jacket. A vacuum pump was used to keep the vacuum level at less than 0.1 atm during the experiment. A ceramic-sealed vacuum feedthrough flange was used to connect the thermocouple wires at the vacuum side and at the air side. There were two transparent quartz windows on vacuum jacket that enable the observation and recording of the two-phase flow regimes inside the test section. The diameter of each window was 7.62 cm. A CCD camera facing one of the quartz windows was used to record flow images, while lighting was provided by a fluorescent light at the other widow.

A 16-channel thermocouple board plugged into the PCI slot of a computer was used to record the temperature measurement. The thermocouple board has built-in cold junction compensation and programmable gain ranges. All the thermocouples were tested and calibrated with boiling nitrogen prior to the chilldown experiments. Video images were monitored and recorded by connecting the CCD camera to the computer with a frame grabber board plugged into the PCI slot of the computer. A commercial software recorded the flow images and also showed the real-time images on the computer screen. It was estimated that the accuracy of the temperature measurements was ± 0.8 °C. The uncertainty of the mass flux was determined by the accuracy of the motor speed, the manufacturing accuracies of the driving screw, the bellows and the test section. The uncertainty of the mass flux was estimated to be about $\pm 6.9\%$.

2.2. Experimental method

During each test, the test section was quenched from the room temperature at about 295 K with the tube oriented horizontally. Three different mass fluxes, namely 3.6 kg/m^{2}s, 7.2 kg/m^{2}s and 10.8 kg/m^{2}s were used. Because of the capacity limit of the bellows, the bellows-driven flow

experiments were conducted only in the film boiling region in which the flow pattern is dispersed flow. Other experiments were performed with gravity-driven flow to investigate the entire chilldown process. In this gravity-driven experiment, a reservoir tank placed above the test section and maintained at a constant liquid level was used to generate the flow. Flow images taken during the chilldown process were analyzed to estimate the mass flux for the gravity-driven experiments. The mass flux was in the range of 18–23 kg/m^2 s.

2.3. Data reduction

Most of the previous quenching tests were conducted for a vertical flow, in which the axisymmetric assumption is generally held. Further with the lumped-system assumption, which is valid only when the Biot number is less than about 0.1, the wall heat flux was directly computed by the temperature–time slope from the cooling data [7,14]. However, the axisymmetric assumption is not valid for a horizontal tube due to the stratified nature of the flow. A comparison between the heat fluxes based on a 2D heat transfer model [15], which considers the axial heat conduction, with those obtained by neglecting the axial conduction was given by Cheng and Ragheb [16]. The comparison for the copper test section showed that the two mid-plane boiling curves are approximately the same and the net axial conduction at the mid-section is negligibly small. In our experiments, the measured axial temperature gradient was relatively small and also the thermal conductivity of the glass is much smaller than that of the copper used by Cheng and Ragheb [16], therefore the axial heat conduction along the test section was neglected in the heat flux calculation.

In order to calculate the local heat transfer data from the measured temperature profiles, a transient energy balance with temperature variations only in the radial direction was performed on the control volume of a thin slice that contains a pair of the bottom inner and outer thermocouples. The circumferential angular conduction of heat into the control volume was evaluated by assuming a linear temperature profile between the upper and bottom thermocouples. Heat transfer due to radiation from a vacuum jacket, natural convection inside the vacuum jacket and circumferential conduction were included by the measured temperatures. The transient energy balance conduction equation was solved numerically using the measured inner and outer temperature data as the boundary conditions. The transient heat flux was then evaluated using the numerically solved temperature profile.

3. Experimental results

3.1. Gravity-driven flow experiment

Typical temperature transients measured at the inlet and outlet of the test section are shown in Fig. 3. It is noted that

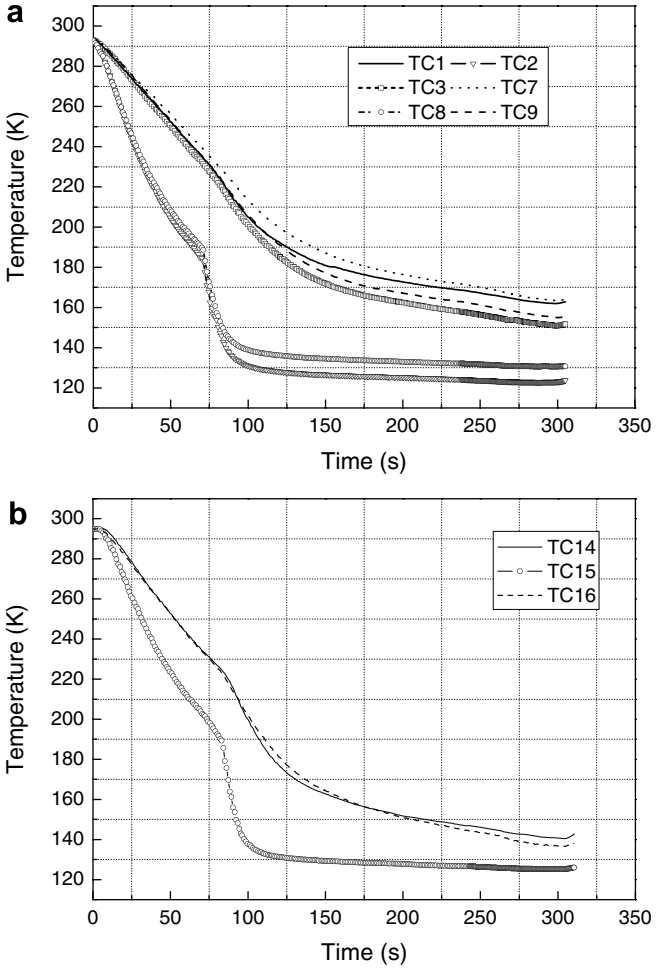

Fig. 3. Transient wall temperature profiles at different axial location in gravity-driven experiments: (a) inlet part; and (b) outlet part.

thermocouples 7, 8, and 9 are located on the outer surface of the tube in Section 2 as shown in Fig. 2. During a chilldown process, most of the liquid nitrogen was found settled in the bottom of the test section, therefore the boiling regime was determined by the characteristics of the heat flux at the tube bottom surface. A typical transient heat flux profile during the chilldown on the bottom of the tube at the outlet cross section is shown in Fig. 4a. As shown in this figure, the heat flux first increases due to the transient effect; after reaching a peak value, the heat flux decreases gradually with decreasing wall superheat and then reaches the minimum heat flux $q''_{\min}$. Before the minimum heat flux point the boiling regime is film boiling. The liquid begins to rewet the bottom wall after the minimum heat flux is reached and then the transition boiling regime begins with a sharp increase in the heat flux, while the maximum or critical heat flux $q''_{\max}$ denotes the beginning of the nucleate boiling. Fig. 4b illustrates the bottom wall heat flux as a function of time.

Here we should point out that in most of the previous quenching experiments, the film boiling heat flux was reported as either being kept at a relatively constant value [9,16], or it decreased as the test section was chilled down

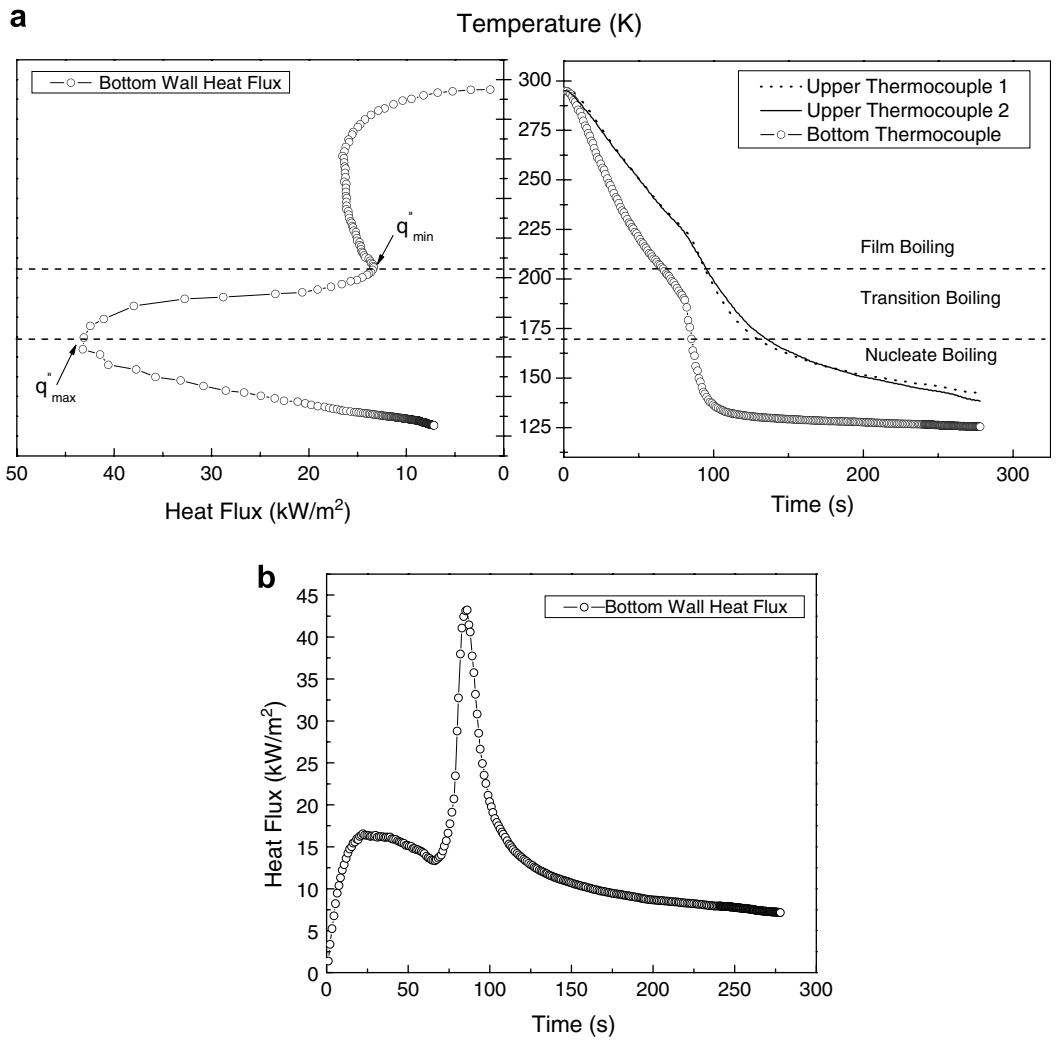

Fig. 4. Typical bottom wall heat flux at outlet cross section in gravity-driven experiments: (a) transient wall temperature profiles and heat flux as a function of wall temperature; and (b) heat flux as a function of time.

[6,14]. In our experiments, however, the local heat flux first increases in a relatively short period, then decreases gradually. This is consistent with the transient nature of the experiments. Generally the heat flux rising period is expected to be shorter at a higher mass flux while keeping the other conditions unchanged. The mass fluxes in previous investigations were much larger, which therefore associate with extremely shorter times of rising heat fluxes in the film boiling regime, than those in our experiments. This might be the reason that the period of rising heat flux was not reported before.

Different flow regimes during the chilldown process are shown in Fig. 5. In the beginning of the film boiling region (Fig. 5a), the flow pattern is basically a dispersed flow, in which the liquid phase is dispersed as drops within a continuous vapor phase. The void fraction of the two-phase flow decreases as the tube is chilled down, and long liquid filaments, separated from wall by a thin vapor film, are observed to flow along the tube bottom. In the film boiling region, heat is primarily transferred from the wall by conduction through the vapor film to evaporate the liquid filaments that are settled on the bottom surface and heat is also transferred from the wall by convection to the vapor phase where there is no liquid filament around.

Once the bottom wall temperature has been reduced substantially and is low enough, transient boiling, which is characterized by intermittent liquid–wall contact and violent bubble generation, is observed as shown in Fig. 5b. Shortly after the transient boiling, a continuous liquid–wall contact is established and the liquid nitrogen began to pile up on the bottom wall surface. The prevailing boiling regime is then nucleate boiling and the flow pattern is stratified flow or wavy flow (Fig. 5c).

3.2. Bellows-driven constant flow rate experiments

The bellows-driven flow experiments were conducted within the film boiling regime. Because of the low mass flux range of the experiments, the flow pattern was dispersed flow. In the early stage film boiling, the wall superheat is

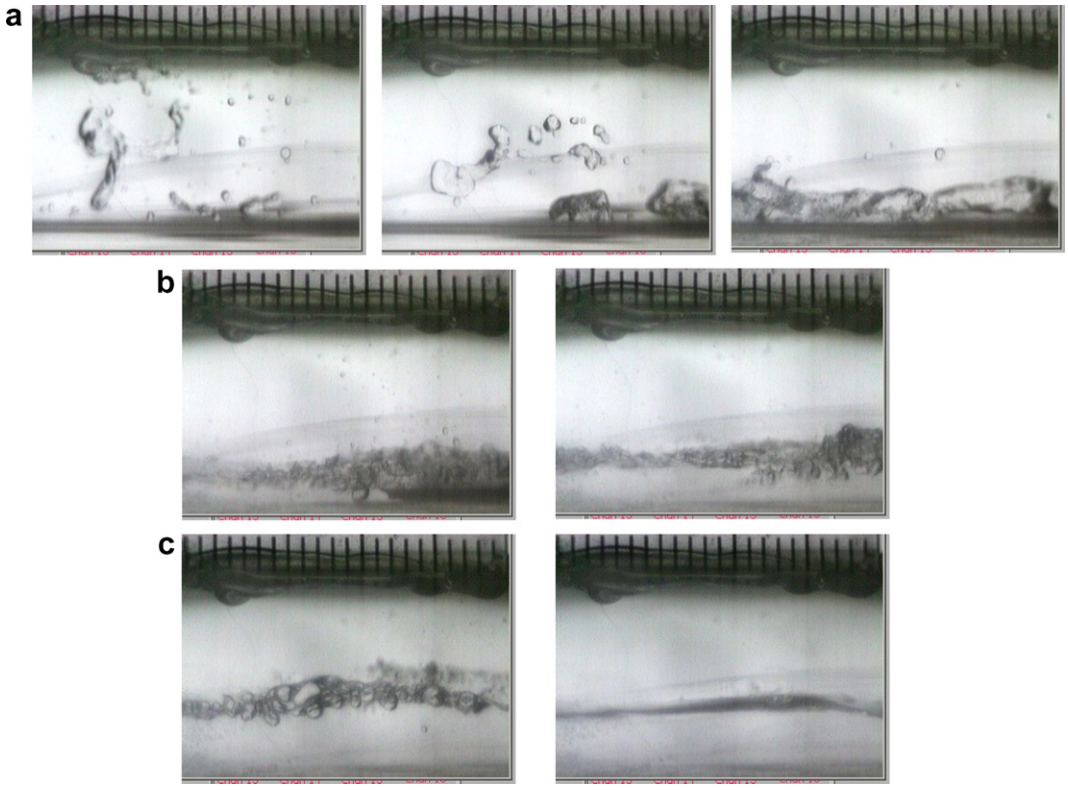

Fig. 5. Flow visualizations of gravity-driven experiment: (a) film boiling region; (b) transition boiling region; and (c) nucleate boiling region.

high and the repulsive force, which is due to fast evaporation or flashing, is very strong. The visualization results showed that when the chilldown is initiated, most droplets are small and near spherical. They are bouncing back and forth on the bottom wall while traveling downstream. As the wall temperature decreases, the liquid droplets tend to form filament shapes and settle down on the bottom of the test section. Typical liquid filament images at different mass fluxes are shown in Fig. 6. Generally, the thickness of the liquid filaments does not change much as the test section is chilled down at different mass fluxes, however, the length of the filaments increases with increasing mass flux and decreasing wall temperature.

The statistic feature of the filaments shows that thickness of the filaments has very limited increase with increasing mass flux and does not present a strong correlation with the wall temperature; while the length of the filaments, however, is more scattered at higher mass fluxes and lower wall temperatures. In other wards, the probability of observing a longer liquid filament is better at a higher mass flux and lower wall temperature.

A summarization of the drop–wall interaction from several experiments was given by Ganić and Rohsenow [6]. They listed the most frequently observed states of drop–wall interaction and the sequence as the wall is cooled down. Current observations generally agree with their summarization.

The temperature profiles measured from the embedded thermocouples at inlet and outlet sections with different mass fluxes are shown in Figs. 7 and 8, respectively. It is obvious that the bottom wall of the test section was chilled down more quickly, because most of the liquid phase was confined at the bottom. The temperature difference between the bottom and the top of the test section was found to increase with increasing mass flux at each cross section. The quality of the two-phase flow generally increases along the test section, consequently the temperature difference between the top and bottom wall is expected to be smaller at further downstream locations. This is confirmed by comparing Fig. 7 with Fig. 8.

The calculated middle section bottom wall heat fluxes under different mass fluxes are shown in Fig. 9a as a function of the local wall temperature. The bottom heat flux first increases during the initial stage when the test section starts to be chilled down, and then decreases gradually with decreasing wall temperature.

Fig. 9b shows the local heat fluxes at three circumferential locations in the middle section as a function of local wall temperature under a mass flux of 7.2 kg/m^2s. It is found that the two heat fluxes at the upper portion of the cross section increase at the beginning of the chilldown process, and then maintain at almost constant values. The heat fluxes at the upper portion of the test section are much smaller than the bottom heat flux in a wide wall temperature range. The reason is that the upper wall losses heat mainly by convection to the superheated vapor, while the main heat transfer mechanism at the bottom is film boiling, which is more efficient than convection.

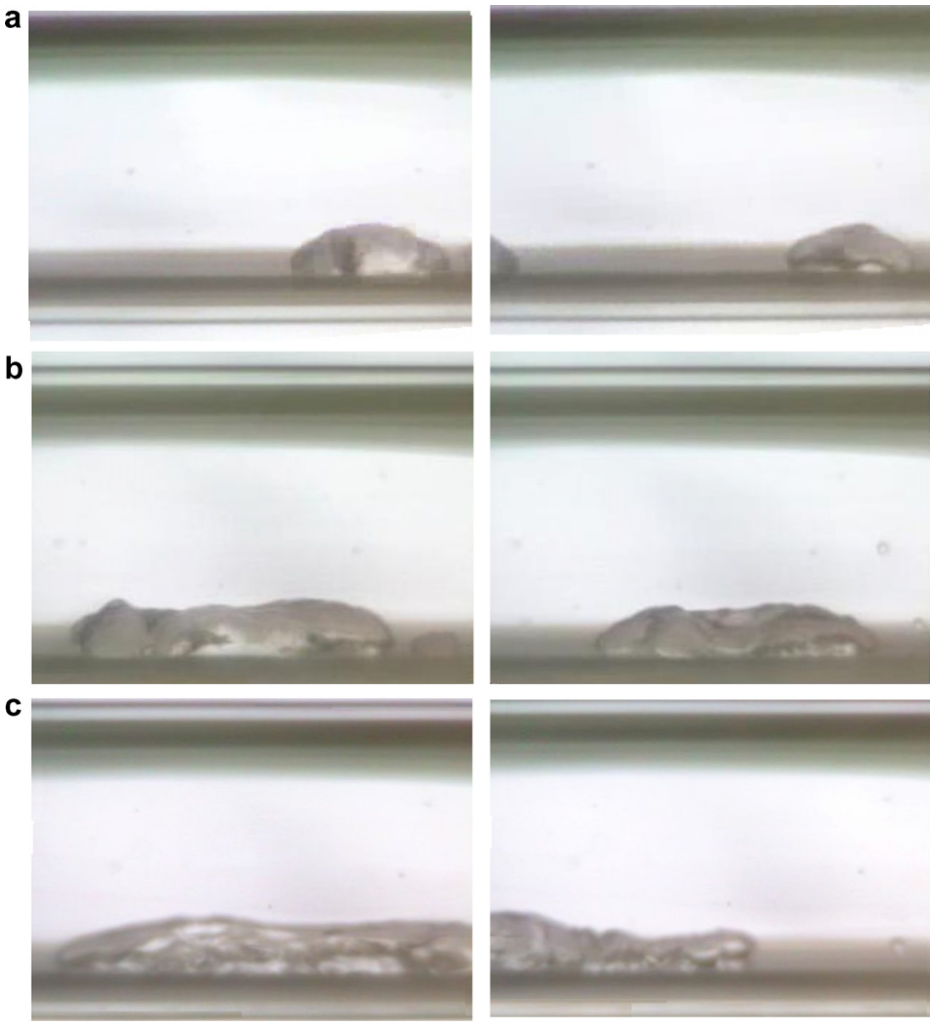

Fig. 6. Typical flow images under different mass flux: (a) mass flux of 3.6 kg/m^{2}s; (b) mass flux of 7.2 kg/m^{2}s; and (c) mass flux of 10.8 kg/m^{2}s.

4. Phenomenological model

The heat transfer mechanism of dispersed flow boiling is very complicated. It is widely accepted that there exists a significant thermodynamic non-equilibrium condition between the vapor phase and the liquid phase [4,17–20]. A model for the vertical dispersed flow boiling suggested by Koizumi et al. [18] and Chung and Olafsson [19] assumed that heat transfer takes place in steps: from the wall to the vapor and then from the vapor to the droplets suspended in the stream; and from the wall to the droplets in contact with the wall. Chen et al. [20] proposed a model for post-CHF region that considered the total heat transfer as a sum of vapor and liquid components and ignored radiation heat transfer to the two-phase mixture.

In our experiment, the condition is highly transient, the inlet quality and vapor superheat are not constant but change with time and mass flux. Therefore a phenomenological model, which also includes information form visualization results, has been developed to analyze the current dispersed flow boiling heat transfer.

4.1. Model description

As mentioned above, the visualization shows that except in the very beginning stage, most of the liquid filaments are flowing along the bottom of the tube. Consequently, in this model the heat transfer mechanisms on the bottom of the test section are considered as the sum from vapor and liquid components, while the heat transfer mechanism at the upper portion of the test section is forced convection to superheated vapor. It has been shown [21,22] that for a wall superheat up to several hundreds Kelvin the radiation heat transfer in post-dryout dispersed flow is generally negligibly small. It is also judged that thermal radiation is minor in our case; therefore radiation heat transfer is ignored in this model.

The heat transfer mechanisms in this model are illustrated in Fig. 10. The bottom wall heat flux is composed of vapor and liquid components. The total bottom wall heat flux can be written as:

$$q''_{\mathrm{b}} = q''_{\mathrm{b1}} F_{\mathrm{L}} + q''_{\mathrm{b2}}(1 - F_{\mathrm{L}}) = q''_{\mathrm{fb}} F_{\mathrm{L}} + q''_{\mathrm{b,con}}(1 - F_{\mathrm{L}}) \qquad (1)$$

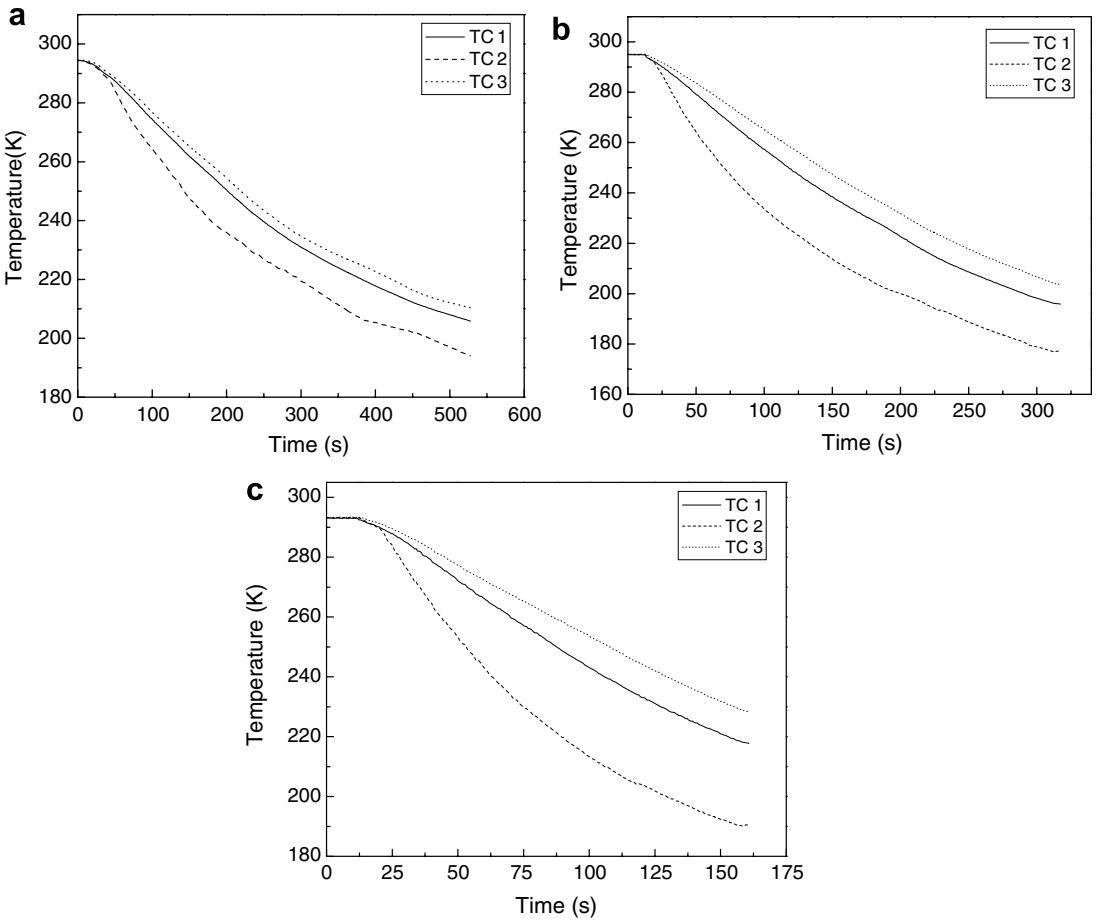

Fig. 7. Temperature profiles of the middle section with different mass flux: (a) mass flux of 3.6 kg/m^{2}s; (b) mass flux of 7.2 kg/m^{2}s; (c) mass flux of 10.8 kg/m^{2}s.

where q''_b is the effective bottom wall heat flux and q''_{fb} is the heat flux from the portion of the bottom surface where a liquid filament is in the vicinity and separated from the wall by a thin vapor film as shown in Fig. 10. Therefore, q''_{fb} is a film boiling heat flux. $q''_{b,con}$ is the heat flux from the bottom surface where there is no liquid filament around, so it is due to pure forced convection to a superheated vapor. F_L is defined as the time averaged fraction of bottom wall surface that is associated with liquid filaments.

The upper wall of the test section is fully in contact with the vapor phase, and the top wall heat flux is described as:

$$\begin{aligned} q''_u &= q''_{u1}F_L + q''_{u2}(1-F_L) \\ &= q''_{u,con1}F_L + q''_{u,con2}(1-F_L) \end{aligned} \quad (2)$$

where q''_u is the effective upper heat flux and $q''_{u,con1}$ is the convective heat flux to the superheated vapor for the portion that is directly opposite to the bottom portion that is associated with liquid filaments as shown in Fig. 10. $q''_{u,con2}$ is therefore for the portion that is directly opposite to the bottom portion that is not associated with liquid filaments. Because of symmetry, the same $q''_{u,con2}$ and $q''_{b,con}$ are considered equal. We note that $q''_{u,con1}$ and $q''_{u,con2}$ are different due to different bulk vapor velocities in their respective sections.

As an idealization, the liquid filaments are modeled as half cylinders in a film boiling state and they move along the bottom of the tube. The filaments are at the saturation temperature and separated from the tube wall by a thin vapor film. Heat transferred to the liquid filament is assumed primarily by conduction across the thin vapor film. Assuming a linear temperature profile exists in the vapor film, the film boiling heat flux can be evaluated as:

$$q''_{fb} = k_g \frac{\Delta T_w}{\delta} \quad (3)$$

where ΔT_w, δ, and k_g are the bottom wall superheat, vapor film thickness and thermal conductivity of the gas in vapor film, respectively.

Generally, the vapor film thickness varies circumferentially in one cross-section. However, Chan [23] showed that for a stable film boiling inside horizontal tubes, the thickness of the vapor film remains essentially constant over a relatively long distance from the bottom of the tube. Therefore the bottom film thickness δ_0 is used to evaluate the film boiling heat flux at the bottom where the experimental measurements are performed. A correlation for the bottom

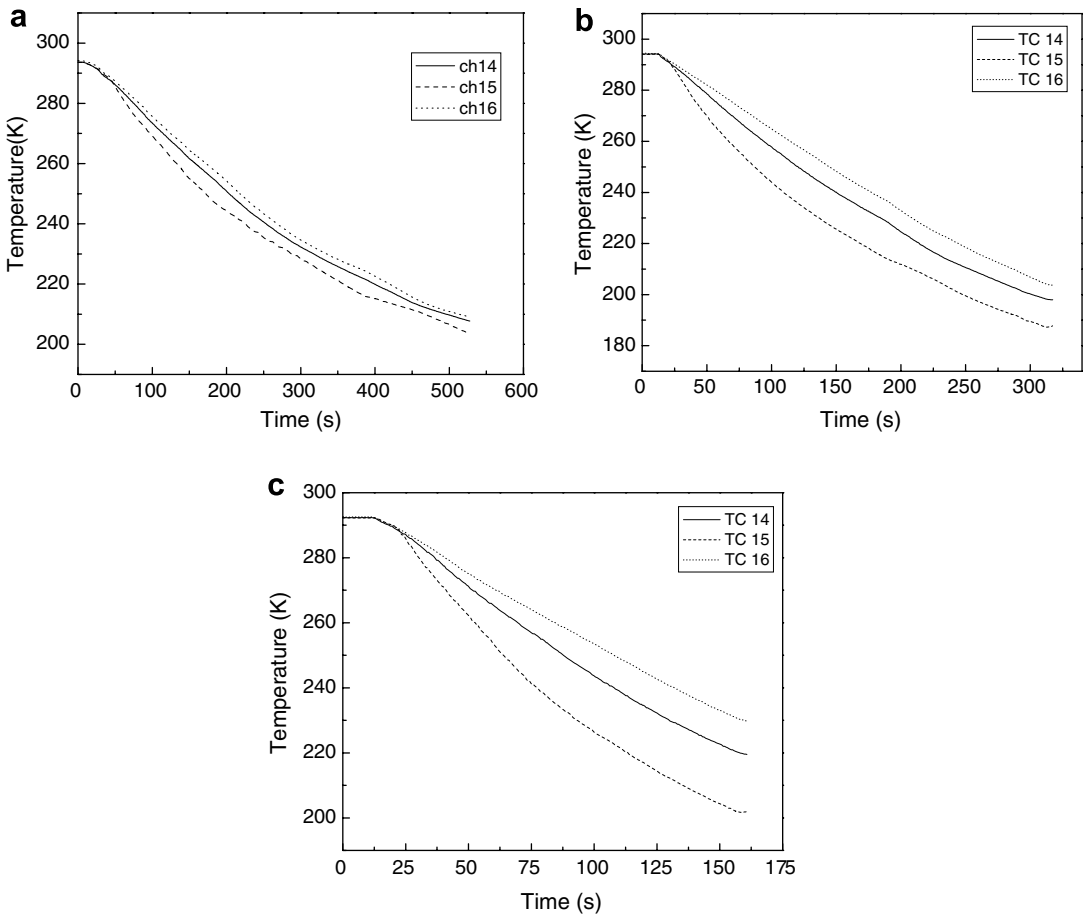

Fig. 8. Temperature profiles of the outlet section with different mass flux: (a) mass flux of 3.6 kg/m^{2}s; (b) mass flux of 7.2 kg/m^{2}s; (c) mass flux of 10.8 kg/m^{2}s.

vapor film thickness δ_0 was given by Chan [23]. In our calculation, the interfacial shear stress was modified and bottom film thickness is obtained as:

$$\delta_0 = 1.189\left[\left(\frac{R}{g\rho_l\rho_g}\right)\left(\frac{k_g\Delta T_w}{h'_{lg}}\right)^2\right]^{\frac{1}{4}} \tag{4}$$

where R is the tube radius; g is gravitational acceleration constant; ρ_l and ρ_g are the densities of liquid phase and gas in vapor film, respectively. While h'_{lg} is defined as the latent heat plus vapor sensible heat content:

$$h'_{lg} = h_{lg} + 0.5C_{pg}\Delta T_w \tag{5}$$

in which h_{lg} is latent heat of evaporation, C_{pg} is specific heat of the gas in the vapor film. It should be noted that in the above equations, all the thermodynamic properties of the gas in the vapor film are evaluated at an average film temperature given by:

$$T_g = 0.5(T_w + T_{sat}) \tag{6}$$

The fraction of liquid filament associated area F_L is expected to increase with increasing mass flux and decreasing wall temperature. The transient liquid fraction in each recorded frame is widely scattered. Therefore F_L is calculated by averaging over a certain time period, the result is shown in Fig. 11a as a function of bottom wall temperature. As the wall temperature decreases, F_L increases more quickly with a higher mass flux. The fitted linear curves in Fig. 11a are used in the model calculation.

Kao et al. [24] suggested that for film boiling flow the transition to turbulence in the vapor flow is almost immediately downstream from the origin of the film boiling region. Therefore, the forced convective heat transfer to the vapor phase is evaluated by the Dittus–Boelter correlation as:

$$q''_{con} = 0.023\frac{k_v}{D}Re_D^{0.8}Pr^{0.4}(T_w - T_v) \tag{7}$$

in which k_v is the vapor phase thermal conductivity; D is the hydraulic diameter of the vapor flow; Re_D is Reynolds number; Pr is the vapor Prandtl number; T_w and T_v are the wall temperature and balk vapor phase temperature, respectively. It is noted that both $q''_{u,con1}$ and $q''_{u,con2}$ are evaluated using Eq. (7), the difference is that each is evaluated based on the respective bulk vapor velocity in its section as shown in Fig. 10.

As mentioned before, the two phases are in thermodynamic non-equilibrium for dispersed flow film boiling.

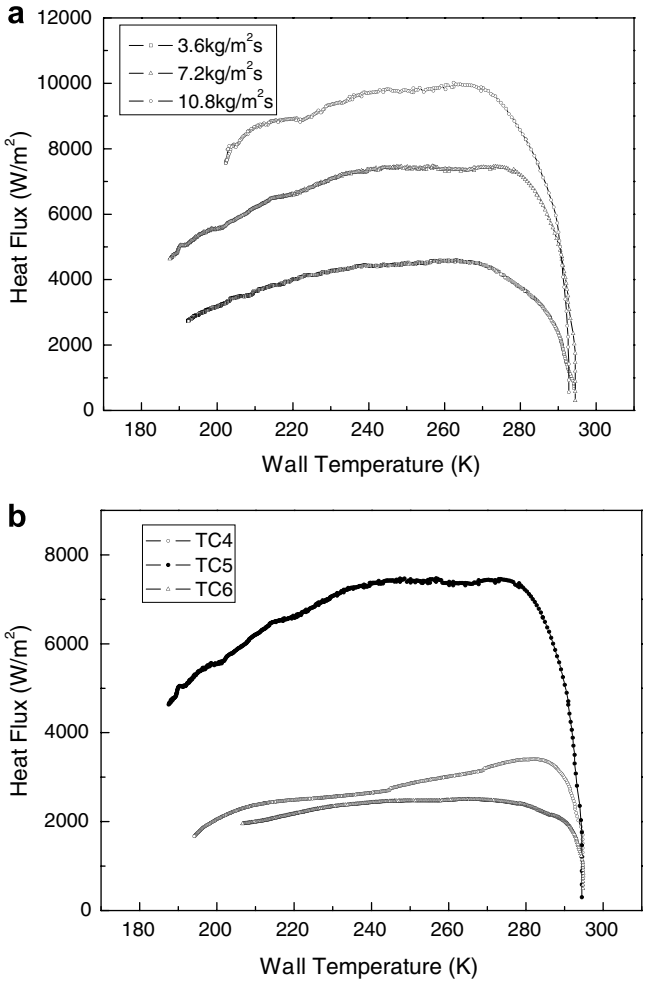

Fig. 9. Wall heat flux in dispersed flow film boiling: (a) middle section bottom wall heat flux under different mass flux; and (b) middle section local wall heat flux under a mass flux of 7.2 kg/m^{2}s.

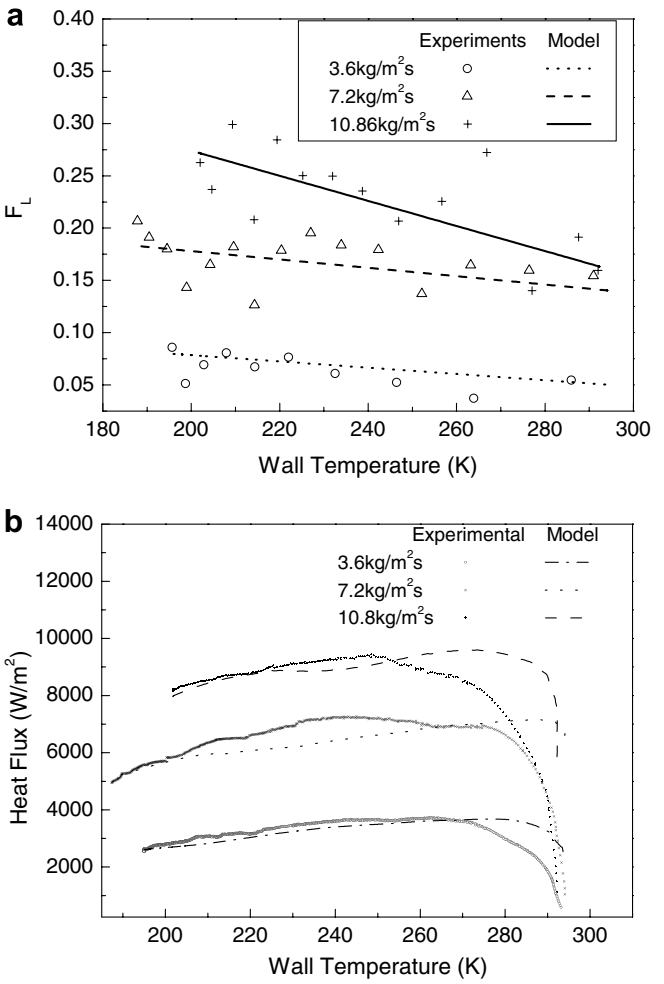

Fig. 11. (a) Liquid contact fraction at different wall temperature and mass flux; and (b) comparison between experimental and model results of the bottom wall heat flux.

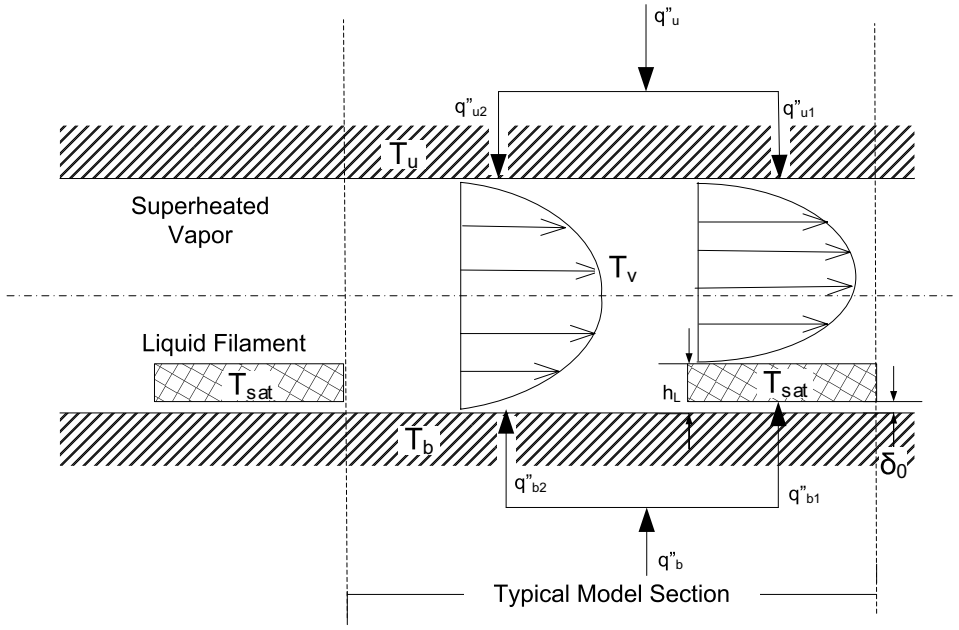

Fig. 10. Description of the heat transfer mechanism under horizontal dispersed flow condition.

The vapor phase could be highly superheated. Because the upper wall heat flux is described as containing only convective heat transfer in this model, the vapor phase temperature can then be calculated by matching the measured upper wall heat flux. With a known vapor phase temperature, the bottom heat flux can be calculated from Eqs. (2), (3) and (7).

4.2. Model evaluation and discussion

The phenomenological model described above permits evaluation of bottom wall heat flux with a known upper wall heat flux. Fig. 11b compares the experimental results with the model prediction for the bottom wall heat flux. It is seen that the model over predicts the heat fluxes in the beginning stage of chilldown where the wall temperatures are high, after that the model is reasonably accurate. Since the flow visualization shows that in the beginning stage the liquid pieces bounce back and forth from the wall rather than settle down on the bottom wall, therefore the above film boiling model with a stable liquid filament in the wall vicinity can not catch the entire physics for the beginning period. Because of the much higher heat flux for a stable film boiling condition than that of bouncing liquid filaments, the current model over-predicts the heat transfer.

5. Conclusions

Cryogenic chilldown process under a low flow rate condition has been studied experimentally. In the gravity-driven flow, the bottom part of the horizontal test section is quenched first, and then liquid nitrogen begins to accumulate on the bottom portion of the test section. The three regimes of the boiling curve are defined according to the bottom wall heat flux and confirmed by the visualization results.

In the current experiment condition, the flow pattern under the film boiling condition is dispersed flow. Visualization results show that most of the liquid phase cannot touch the bottom wall in the early stage, as the wall temperature decreases, liquid filaments are found to settle on the bottom of the test section.

In the film boiling regime, the local heat flux first increases in a relatively short period and then decreases with decreasing wall temperature. The length of the liquid filaments generally increases with increasing mass flux and decreasing wall temperature, while the thickness of the liquid filaments was found to have a very limited increase with increasing mass flux and does not show a strong correlation with the wall temperature. The fraction of the bottom wall surface that is associated with liquid filaments in the vicinity increases with increasing mass flux and decreasing wall temperature. Also this fraction increases more quickly with a higher mass flux.

A phenomenological model was developed and used to predict the bottom wall heat flux with known upper wall heat flux. It is found that the model over predicts the heat flux during the beginning stage of the chilldown process, while the prediction for the rest of the heat fluxes agrees well with the experimental data.

Acknowledgements

This research was supported by the NASA Hydrogen Research for Spaceport and Space Based Applications at the University of Florida (Grant number NAG3-2930). Dr. N.T. Van Dresar of NASA Glenn Research Center provided many insightful comments and discussion. The support by the Andrew H. Hines, Jr./Progress Energy Endowment Fund is also acknowledged.

References

[1] J.C. Burke, W.R. Byrnes, A.H. Post, F.E. Ruccia, Pressure cooldown of cryogenic transfer lines, Adv. Cryogenic Eng. 4 (1960) 378–394.
[2] J.C. Bronson, F.J. Edeskuty, J.H. Fretwell, E.F. Hammel, W.E. Keller, K.L. Meier, A.F. Schuch, W.L. Willis, Problems in cool-down of cryogenic systems, Adv. Cryogenic Eng. 7 (1962) 198–205.
[3] B.N. Antar, F.G. Collins, Flow boiling during quenching in low gravity environment, Int. J. Microgravity Sci. Technol. 3 (1997) 18–128.
[4] W.F. Laverty, W.M. Rohsenow, Film boiling of saturated nitrogen flowing in a vertical tube, ASME J. Heat Transfer 91 (1967) 90–98.
[5] O.C. Iloeje, D.N. Plummer, W.M. Rohsenow, P. Griffith, An investigation of the collapse and surface rewet in film boiling in forced vertical flow, ASME J. Heat Transfer 97 (1975) 166–172.
[6] E.N. Ganić, W.M. Rohsenow, Dispersed flow heat transfer, Int. J. Heat Mass Transfer 20 (1977) 855–866.
[7] O.C. Iloeje, D.N. Plummer, W.M. Rohsenow, P. Griffith, Effects of mass flux, flow quality, thermal and surface properties of materials on rewet of dispersed flow film boiling, ASME J. Heat Transfer 104 (1982) 304–308.
[8] A.M.C. Chan, S. Banerjee, Refilling and rewetting of a hot horizontal tube Part I: experiments, ASME J. Heat Transfer 103 (1981) 281–286.
[9] C.J. Westbye, M. Kawaji, B.N. Antar, Boiling heat transfer in the quenching of a hot tube under microgravity, J. Thermophys. Heat Transfer 9 (1995) 302–307.
[10] C.S. Lin, N.T. Van Dresar, M.M. Hasan, Pressure control analysis of cryogenic storage systems, J. Propul. Power 20 (2004) 480–485.
[11] N.T. Van Dresar, J.D. Siegwarth, Near-horizontal, two-phase flow patterns of nitrogen and hydrogen at low mass and heat flux, NASA TP 2001-210380, 2001.
[12] N.T. Van Dresar, J.D. Siegwarth, M.M. Hasan, Convective heat transfer coefficients for near-horizontal two-phase flow of nitrogen and hydrogen at low mass and heat flux, Cryogenics 41 (2002) 805–811.
[13] C.J. Swanson, R.J. Donnelly, G.G. Ihas, Turbulent pipe flow of He I and He II, Physica B 284–288 (2000) 77–78.
[14] A.E. Bergles, W.G. Thompson, The relationship of quench data to steady-state pool boiling data, Int. J. Heat Mass Transfer 13 (1970) 55–68.
[15] S.C. Cheng, Transition boiling curves generated from quenching experiments using a two dimensional model, Lett. Heat Mass Transfer 5 (1978) 391–403.
[16] S.C. Cheng, H. Ragheb, Transition boiling data of water on Inconel surface under forced convective conditions, Int. J. Multiphase Flow 5 (1979) 281–291.
[17] R.A. Nelson, Forced-convective post-CHF heat transfer and quenching, ASME J. Heat Transfer 104 (1982) 48–54.
[18] Y. Koizumi, T. Ueda, H. Tanaka, Post dryout heat transfer to R-113 upward flow in a vertical tube, Int. J. Heat Mass Transfer 22 (1978) 669–678.

[19] J.N. Chung, S.I. Olafsson, Two-phase droplet flow convective and radiative heat transfer, Int. J. Heat Mass Transfer 27 (1984) 901–910.
[20] J.C. Chen, F.T. Ozkaynak, R.K. Sundaram, Vapor heat transfer in post-CHF region including effect of thermodynamic non-equilibrium, Nucl. Eng. Des. 51 (1979) 143–155.
[21] W.X. Tian, S.Z. Qiu, D.N. Jia, Investigations on post-dryout heat transfer in bilaterally heated annular channels, Ann. Nucl. Energy 33 (2006) 189–197.
[22] Y.J. Guo, K. Mishima, A non-equilibrium mechanistic heat transfer model for post-dryout dispersed flow regime, Exp. Ther. Fluid Sci. 26 (2002) 861–869.
[23] A.M.C. Chan, Stratified flow film boiling inside horizontal tubes, ASME J. Heat Transfer 117 (1995) 179–184.
[24] H.S. Kao, C.D. Morgan, M. Crawford, J.B. Jones, Stability analysis of film boiling, AIChE Symposium Series, 68, 1972, pp. 147–155.